Infrared image detail enhancement based on the gradient field specification

Wenda Zhao,[1,2] Zhijun Xu,[1,*] Jian Zhao,[1] Fan Zhao,[1,2] and Xizhen Han[1]

[1]Changchun Institute of Optics, Fine Mechanics and Physics, Chinese Academy of Sciences, 130033 Changchun, China

[2]University of Chinese Academy of Sciences, 100049 Beijing, China

*Corresponding author: xuzj538@ciomp.ac.cn

Received 6 January 2014; revised 7 May 2014; accepted 13 May 2014;
posted 15 May 2014 (Doc. ID 204003); published 23 June 2014

Human vision is sensitive to the changes of local image details, which are actually image gradients. To enhance faint infrared image details, this article proposes a gradient field specification algorithm. First we define the image gradient field and gradient histogram. Then, by analyzing the characteristics of the gradient histogram, we construct a Gaussian function to obtain the gradient histogram specification and therefore obtain the transform gradient field. In addition, subhistogram equalization is proposed based on the histogram equalization to improve the contrast of infrared images. The experimental results show that the algorithm can effectively improve image contrast and enhance weak infrared image details and edges. As a result, it can give qualified image information for different applications of an infrared image. In addition, it can also be applied to enhance other types of images such as visible, medical, and lunar surface. © 2014 Optical Society of America

OCIS codes: (100.2960) Image analysis; (100.2980) Image enhancement; (100.5010) Pattern recognition.

http://dx.doi.org/10.1364/AO.53.004141

1. Introduction

Infrared images are widely applied in military, scientific, medical, and other fields. However, infrared images have the shortcomings of low contrast and blurred texture details due to nonideal optics and the uneven photosensitive response of an infrared detector, which is caused by the randomness in the process of manufacturing, such as the different effective photosensitivities and the change of semiconductor doping, making the photoelectric conversion curve inconsistent and the dark current uneven. Thus many details are hidden in the dark background and cannot be identified, which affects the application of infrared images. To give qualified image information for applications, it is necessary to enhance the faint details in the dark background of infrared images [1,2].

There are a lot of image enhancement algorithms, such as image contrast enhancement [3,4] and image sharpening [5,6]. To enhance weak details in the dark background, a straightforward idea is to improve the image contrast in the dark background so that details can be revealed. The common algorithms include histogram equalization (HE) and improved algorithms [7–10]. They make the image gray value distributed in the histogram with equivalent probability, which extends the dynamic range of the histogram. However, they easily lead to the combination of small and similar gray values, resulting in the loss of weak information of the image. Another idea is to make the image sharper, so that image details become clear [11–13]. It can effectively enhance the image details in a bright background. However, as for the details in dark background, the effect is not obvious. The histogram specification (HS) method [14–17] can guide the mapping of the gray value through a predetermined function to make the histogram become

1559-128X/14/194141-09$15.00/0

a predetermined shape. If the function is selected properly, the important gray-scale range can be highlighted to reach the purpose of enhancing images. In order to enhance the image texture details effectively, this article will extend HS to the gradient domain of images and use it to transform the image gradient histogram. A similar idea has been used in other aspects of image processing, such as image denoising [18] and image detection [19]. Human vision is sensitive to the change of the local details of images, which are actually the gradients of images. Therefore, we can adjust the image gradient field to enhance image details.

In order to effectively enhance weak image edge textures and improve image contrast, this article presents the infrared image detail enhancement algorithm based on the gradient field specification (GFS). First we construct a Gaussian function to obtain the gradient HS and therefore obtain the enhanced gradient field. Second we use the variational method to rebuild a new image from the gradient field. Third we improve the overall contrast of the new image by combing HE with subhistogram equalization (SHE) transformation. The experimental results show that the algorithm cannot only effectively enhance weak details and edges of the infrared image, but also can be applied to enhance other types of images such as visible, medical, and lunar surface.

This article is organized as follows. In Section 2, we describe the algorithm of infrared image detail enhancement based on GFS. In Section 3, we give experimental results and related discussions, followed by a brief conclusion.

2. Proposed Algorithm

The process of the proposed algorithm is shown in Fig. 1. Each step will be introduced in the following contents.

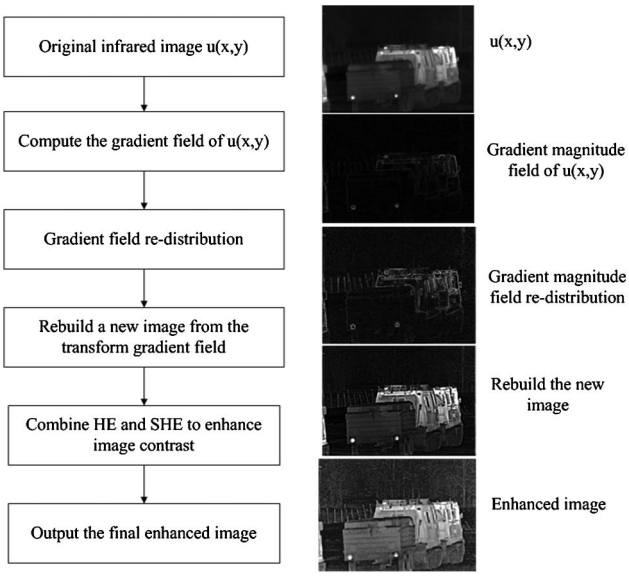

Fig. 1. Overall process of the proposed algorithm.

A. Gradient Histogram Specification

To an infrared image, $u(x,y)[(x,y) \subset \Omega]$, the gradient of the point $p \subset \Omega$ is

$$\nabla u_p = \left[\frac{\partial u_p}{\partial x}, \frac{\partial u_p}{\partial y}\right]. \tag{1}$$

So gradients of each point form a vector field (the gradient field). It reflects the changes of adjacent gray values of each point, where the gradient magnitude indicates the speed of change, and the direction of the gradient indicates the direction of the change of gray value.

The gradient HS method can guide the mapping of the gradient value through a predetermined function to make the gradient histogram become a predetermined shape. The calculation steps are as follows:

1. In accordance with Eq. (2), the gradient value s_k^T, which corresponded with the original gradient value r_k^T, can be calculated as

$$s_k^T = T(r_k^T) = \sum_{i=0}^{k} p(r_i^T) = \sum_{i=0}^{k} \frac{n_i^T}{n^T}, \tag{2}$$

where $0 \le s_k^T \le 1$, $k = 0, 1, \ldots, l-1$, n_i^T indicates the number of pixels whose gradient value is r_i^T, n^T represents the total number of pixels, $p(r_i^T)$ is the probability density of the gradient value, and $T(r_k^T)$ is the sum of probability density.

2. From Eq. (3), the z_k^T, which represents the gradient value of the output image, is transformed to the v_k^T according to the Gaussian function $f(x)$:

$$v_k^T = G(z_k^T) = \sum_{i=0}^{k} f(z_i^T). \tag{3}$$

3. According to the mapping rules of [20], the correspondence relationship $v_k^T \to s_k^T$ can be found and then calculate z_k^T according to Eq. (4):

$$z_k^T = G^{-1}(s_k^T), \tag{4}$$

where G^{-1} represents the inverse transform of G.

Accordingly [21], the gradient value has a direct impact on the visual effect of an image. More specifically, the larger the gradient value, the clearer the image details become. In this article, we apply HS to the image gradient field and therefore enhance the faint image details by varying the gradient histogram. Based on lots of low-contrast infrared images with unclear details, we find that their gradient histogram appears as a slim shape with a sharp peak close to zero [as the $p(x)$ of Fig. 2 shows]. When HS is considered, we need to find an "ideal" function to perform the gradient HS. According to characteristics of the gradient histogram, as mentioned above, we select the Gaussian function as the gradient HS function:

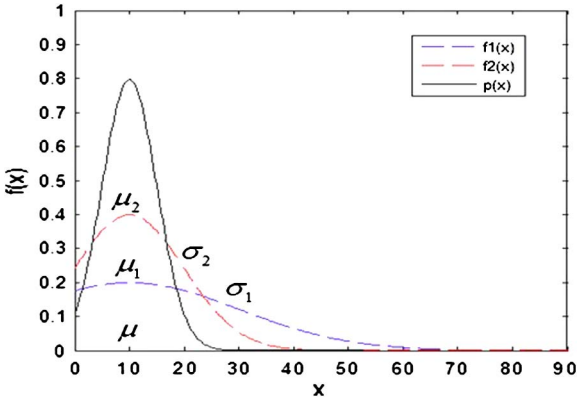

Fig. 2. Graphical illustration of the gradient histogram obtained from the Gaussian function.

$$f(x) = \frac{1}{\sqrt{2\pi}\sigma} e^{\frac{(x-\mu)^2}{2\sigma^2}} \qquad (-\infty < x < +\infty); \tag{5}$$

where $f(x)$ stands for the Gaussian function, x stands for a random variable, and μ and σ are parameters of Gaussian function. The graphical illustration of the gradient histogram $p(x)$ obtained from the Gaussian function $f_1(x)$ and $f_2(x)$ is shown in Fig. 2, where $\mu_1 = \mu_2 = \mu$ and $\sigma_1 > \sigma_2$. In Fig. 2, μ adjusts the position of the Gaussian peak. In general, as σ increases, the curve will become smoother with a more flattened peak. If the peak shape flattens, the gradient value will extend to the direction of the larger value, and the image details will be clarified. We take μ and σ as

$$\mu = \sum_{r^T=0}^{l-1} r^T p(r^T), \tag{6}$$

$$\sigma = \frac{1}{\left\{\beta\left[\sum_{r^T=0}^{l-1} (r^T - \mu)^2 p(r^T)\right]^{1/2}\right\}}, \tag{7}$$

where r^T stands for the image gradient value, l stands for the maximum gradient value, $p(r^T)$ is the probability density function of r^T, and β is a variable, which indicates the size of σ. As Fig. 2 shows, the gradient values of the infrared image are small. And taking μ as the average gradient value, we can make the Gaussian peak fall in the range of small gradient values. If the shape of the gradient histogram is narrow, the variance of gradient values will be smaller, and σ will be greater according to Eq. (7). So, as mentioned above, the peak shape is more flattened. And then the gradient histogram will expand toward the direction of positive infinity. Therefore, image details will become clearer. Here we give an example. Figures 3(a)–3(d) show the original image, the modified image by gradient HS, the enhanced image by HE and SHE only (will be introduced in Section 2.C), and the final enhanced image by the proposed algorithm. Figures 3(e) and 3(f) show the original gradient magnitude field and the transformed gradient amplitude field, respectively. Figures 3(g) and 3(h) are their gradient histogram, where the horizontal axis represents the gradient value, and the vertical axis represents the number of pixels.

The original image gradient histogram in Fig. 3(g) is a narrow single peak, and gradient values are small. Image edge textures are fuzzy, as shown in Figs. 3(a) and 3(e). After the specification based on the Gaussian function, the peak shape becomes gentle, and the gradient values increase, as shown in Fig. 3(h). Corresponding to Figs. 3(b) and 3(f), image edge textures are clear. In Fig. 3(c), image contrast is improved, and the details in the dark background are

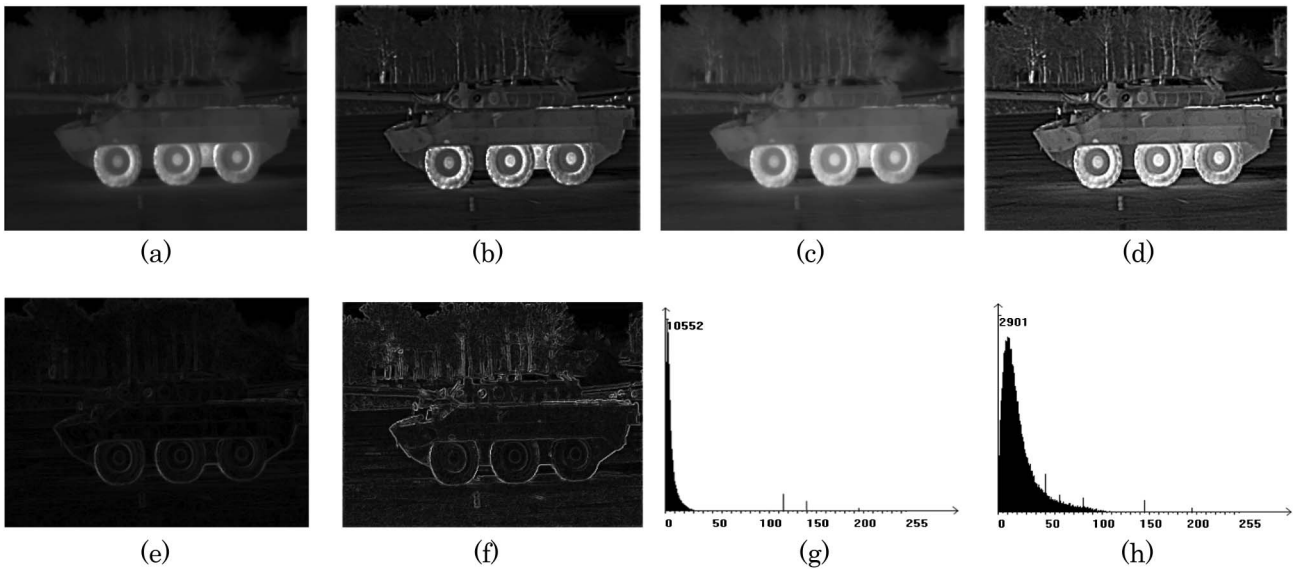

Fig. 3. Gradient magnitude fields and gradient histograms of the armored car. (a) Original image. (b) Modified image by gradient HS. (c) Enhanced image by HE and SHE only. (d) Final enhanced image by the proposed algorithm. (e) Original gradient magnitude field. (f) Transformed gradient amplitude field. (g) Original gradient histogram. (h) Transformed gradient histogram.

revealed. Combining gradient HS with HE and SHE, the final enhanced image is shown in Fig. 3(d). It has a suitable contrast, and texture edges are very clear.

With the Gaussian function, we can use it to guide the gradient histogram transformation. According to the calculation steps above, the $S(|\nabla u_0|)$, which represents the gradient amplitude field after specification, can be calculated. In this notation, u_0 is the original infrared image, ∇ is gradient operator, ∇u_0 is the gradient field of original image, and $|\nabla u_0|$ represents the gradient amplitude field. Define $\mathbf{G}$ as the gradient field after specification:

$$\mathbf{G} = S(|\nabla u_0|) \cdot \frac{\nabla u_0}{|\nabla u_0|}, \tag{8}$$

where $\nabla u_0/|\nabla u_0|$ is to keep the direction of image gradient field unchanged.

B. Rebuild the New Image from the Transform Gradient Field

Now we have obtained the transform gradient field $\mathbf{G}$, and if we find an image u_f: $\Omega \to R$, whose gradient field is equal to $\mathbf{G}$, the image u_f will have clear edge textures. To find the image u_f, an intuitive idea is to solve the equation $\nabla u_f = \mathbf{G}$. However, usually it has no solution because $\mathbf{G}$ constructed from Eq. (8) may not be integrable, and there will not exist an infrared image that has the exact edge texture information as $\mathbf{G}$. A common method for this problem is to find a closest image u_s in the L^2 norm; that is, if $\mathbf{G}$ is the target gradient field, we want the gradient of the solution to have the least-squared error to $\mathbf{G}$.

Using a mathematical formula, it can minimize the following function:

$$F(u_s) = \min\left\{\iint_\Omega |\nabla u_s - \mathbf{G}|^2 \mathrm{d}x\mathrm{d}y\right\}. \tag{9}$$

This article regards Eq. (9) as the GFS model. Using the variational method, the Euler–Lagrange in Eq. (9) is

$$\begin{cases} \Delta u_s = \operatorname{div}\mathbf{G} & \text{on } \Omega \\ \nabla u_s \cdot \vec{n} = \mathbf{G}\cdot\vec{n} = 0 & \text{on } \partial\Omega \end{cases}, \tag{10}$$

where Δ is the Laplace operator, and div is the divergence operator. Assuming that $\mathbf{G}$ on the boundary $\partial\Omega$ is obtained from the source image boundary symmetrical continuation, it is established that $\mathbf{G}\cdot\vec{n} = 0$ on $\partial\Omega$, where $\vec{n}$ is outside the normal vector of Ω. There are a lot of methods to solve the Poisson equation in Eq. (10). Here, according to [21], we adopt a simple iteration method, such as Eq. (11):

$$u_s^{n+1} = u_s^n - \frac{1}{4}(\Delta u_s^n - \operatorname{div}\mathbf{G}), \tag{11}$$

where n represents the number of iterations. The Laplace operator and divergence operator must be discretized appropriately to avoid image displacement. For the Laplacian operator, we reconstruct the new image using forward difference derivatives. And the divergence operator is computed using backward difference derivatives:

$$\begin{aligned}\Delta u_s(i,j) = {} & u_s(i+1,j) + u_s(i-1,j) + u_s(i,j+1) \\ & + u_s(i,j-1) - 4u_s(i,j),\end{aligned} \tag{12}$$

$$\operatorname{div}\mathbf{G} = G_x(i,j) - G_x(i-1,j) + G_y(i,j) - G_y(i,j-1), \tag{13}$$

where $(i,j) \in [0, I-1] \times [0, J-1]$, $\mathbf{G} = (G_x, G_y)$. Combining Eqs. (11)–(13), this integration is done intuitively as follows:

$$u_s^{n+1}(i,j) = u_s^n(i,j) - \frac{1}{4}\left\{\begin{array}{l}[u_s(i+1,j) + u_s(i-1,j) + u_s(i,j+1) + u_s(i,j-1) - 4u_s(i,j)] \\ -[G_x(i,j) - G_x(i-1,j) + G_y(i,j) - G_y(i,j-1)]\end{array}\right\}. \tag{14}$$

The range of these values must sit between [0,255] to be displayed on the computer. Therefore, each iteration should be a reconstrained, iterative form as follows:

$$\begin{cases} u_{\text{temp}} = u_s^n - \frac{1}{4}(\Delta u_s^n - \operatorname{div}\mathbf{G}) \\ u_s^{n+1} = \max\{0, \min(255, u_{\text{temp}})\} \end{cases}. \tag{15}$$

$F(u_s)$ of Eq. (9) may not be satisfied with convexity, so iterations of Eq. (14) may not converge. In image processing, to solve this problem, we usually choose a suitable initial value, hoping to find a meaningful local extreme point. Here we take the input image u as the initial iteration value u_s^0, then the optimal result image from the iteration is the related solution for $F(u_s)$ intuitively. The image reconstruction process, corresponding to part 4 of Fig. 1 (rebuild a new image from the transform gradient field), is shown in Fig. 4.

C. Combine HE and SHE to Enhance Image Contrast

Although the GFS can effectively enhance image edge textures, it still cannot improve the image contrast greatly. As a result, a new method, the SHE

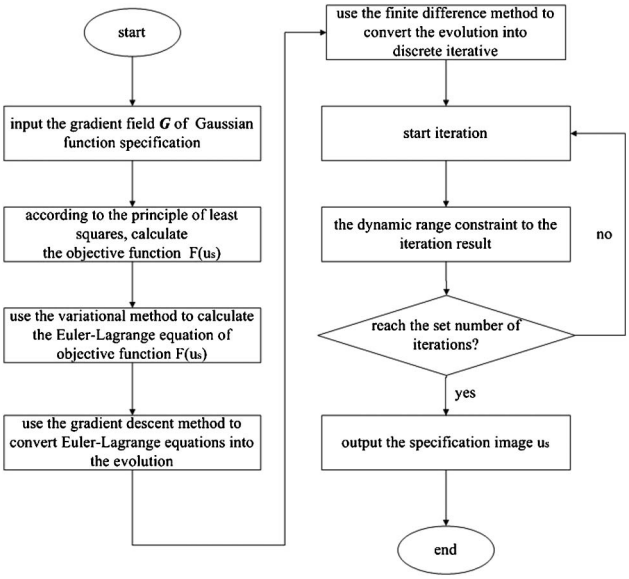

Fig. 4. Flowchart of image reconstruction.

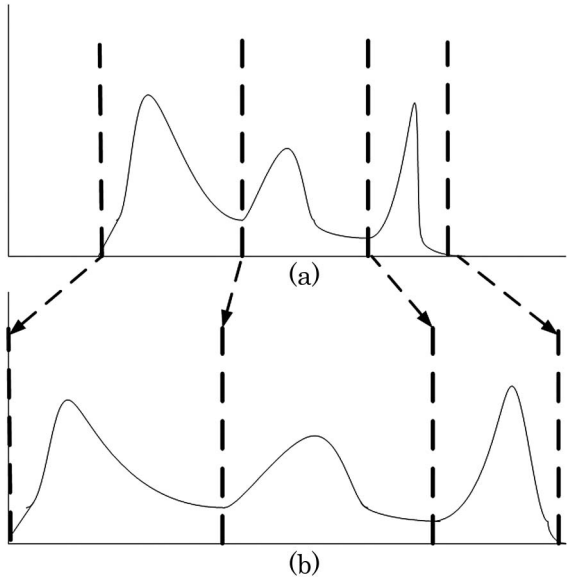

Fig. 5. Subhistogram segmentation schematic diagram. (a) Dividing the histogram based on local minima. (b) Subhistogram expansion.

transform algorithm based on HE, is proposed. HE can effectively improve the image contrast, but is easy to produce the overenhancement. To prevent the overenhancement, we will divide the histogram into several subhistograms, so that none of them has any dominating portion. Then, for each subhistogram of the image u_s, which is reconstructed from the transform gradient field $\mathbf{G}$, we do HE to enhance the contrast well. Combining HE and SHE, the brightness of the whole image is adjusted more uniformly and will not appear the overenhancement phenomenon of HE.

We divide the histogram of image u_s based on local minima [22]. First we use a 1D smoothing filter with size 1×3 on the histogram to get rid of insignificant minima. If there are $(n+1)$ gray levels $d_0, d_1, \ldots, d_n$, which correspond to $(n+1)$ local minima in the image histogram, we define the histogram components of the gray-level range $[d_0, d_1]$ as the first subhistogram, the gray-level range $[d_1+1, d_2]$ as the second subhistogram, and so on. Figure 5(a) is the illustration of such partitioning approach.

In order to achieve the purpose of improving image u_s contrast, the subhistogram should be extended, and the subhistogram i is extended as Eqs. (16) and (17):

$$a_i = (d_i - d_{i-1}) \log\left(\sum_{k=d_{i-1}+1}^{d_i} n_k\right), \tag{16}$$

$$R_i = 255 \times \frac{a_i}{\sum_{k=1}^{n} a_k}, \tag{17}$$

where a_i is the extended coefficient of subhistogram i, n_k means the number of k gray levels, d_i is the gray level that corresponds to local minima i in the image histogram, and R_i is the extended dynamic gray-level range of subhistogram i. If the gray-level range of subhistogram i is extended to $[i_{\text{start}}, i_{\text{end}}]$, then $i_{\text{start}} = (i-1)_{\text{end}} + 1$ and $i_{\text{end}} = i_{\text{start}} + R_i$. The illustration of subhistogram expansion is presented in Fig. 5(b).

At last, we do HE for each subhistogram of the reconstructed image u_s (see Sections 2.A and 2.B) to improve the image contrast. SHE are calculated as follows:

$$\begin{cases} s_{k_i} = R_i \cdot \sum_{j=(i-1)_{\text{end}}+1}^{k_i} \frac{n_j}{n_i} & i = 1 \\ s_{k_i} = \sum_{m=1}^{i-1} R_m + R_i \cdot \sum_{j=(i-1)_{\text{end}}+1}^{k_i} \frac{n_j}{n_i} & i \geq 2 \end{cases}, \tag{18}$$

where k_i is the gray level of the extended subhistogram i, and $k_i \in [(i-1)_{\text{end}} + 1, i_{\text{start}} + R_i]$, s_{k_i} means the SHE gray level value corresponding with k gray level; n_i is the total number pixels of the extended subhistogram i, n_j means the number of gray-level j, and m is the number of the subhistogram.

By dividing the histogram of the reconstructed image u_s into several subhistograms and doing HE for each subhistogram, the image contrast is improved greatly, and weak details in the dark background are enhanced effectively.

3. Experimental Results

In Section 2.A, the selection of β is particularly important, which is directly related to image enhancement effect. In Eq. (7), along with the reduction of β, σ will increase, and the curve will become smoother with a more flattened peak, as shown in Fig. 2. Then the modified gradient value will get bigger, and the image texture edge becomes clearer. But if β is too small, the image will be excessively sharpened. In order to make the GFS image have good visual effect, β should be within a range. Here we give a set of modified images when β are taking different values, as

Fig. 6. Modified images comparison with different β. (a) $\beta = 2.5$, (b) $\beta = 2.0$, (c) $\beta = 1.5$, (d) $\beta = 1.0$.

shown in Fig. 6. The original image is shown in Fig. 3(a).

In Fig. 6, with the decrease of β, the modified image texture edges are becoming increasingly clear. When $\beta = 2.5$, the image texture edges have been enhanced, but not very clear as shown in Fig. 6(a); when $\beta = 1.0$, the image texture edges are very clear, but the whole image looks too sharpened, as shown in Fig. 6(d). In Figs. 6(b) and 6(c), the image has a good visual effect, and texture details are very clear. Therefore, this article takes $\beta = 1.5$–2.0.

To verify the effectiveness of the algorithm, comparing it with plateau HE [7], double plateaus HE [8], and multiscale new top-hat transform [11], we conduct a lot of experiments. Here are some experimental results.

Figure 7(a) is an infrared original image with a dark background and a bright truck in the center. Using plateau HE and double plateaus HE, the image contrast is improved and does not appear to be overenhanced. However, the edge textures of details in the background are still unclear. Figure 7(d) is the result of multiscale new top-hat transform. The image texture edges are clear, but the contrast is low. The result of the proposed algorithm is shown in Fig. 7(e). It effectively improves the image contrast, and the edge textures of details are clear such as the roadside fence and trees.

Figure 8(a) is another infrared original image, and textures on the door are unclear because of the dark background. Using plateau HE and double plateaus HE, the image contrast is improved, and the textures on the door in the background are clearer than in Fig. 8(a). Figure 8(d) is the result of a multiscale new top-hat transform. The image texture edges in the bright background are clear, but the contrast in the dark background is low. The image of the algorithm is shown in Fig. 8(e). The texture edges in the bright and dark backgrounds are very clear.

Figure 9(a) is a low dynamic range infrared image because of the mass fog. Plateau HE and double plateaus HE expand the dynamic range, and most of the details are displayed. A multiscale new top-hat transform sharpens the image, and the details are clearer than in Fig. 9(a). Compared with the previous three methods, the image enhanced by the proposed algorithm has the most reasonable dynamic range and the clearest details.

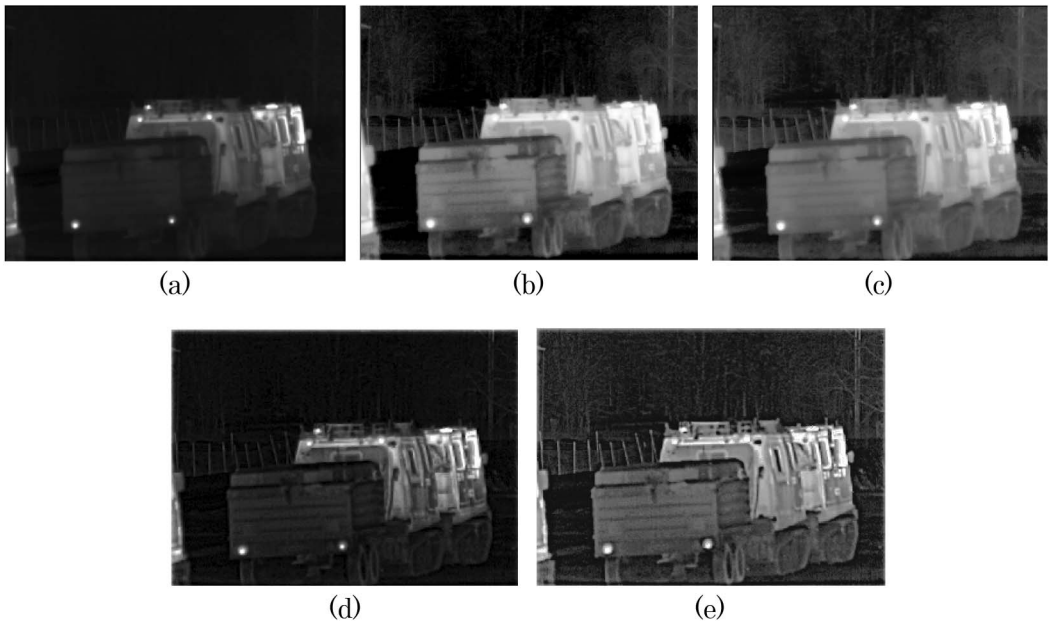

Fig. 7. Experimental results comparison of different algorithms. (a) Original infrared image. (b) Plateau HE. (c) Double plateaus HE. (d) Multiscale new top-hat transform. (e) Proposed algorithm.

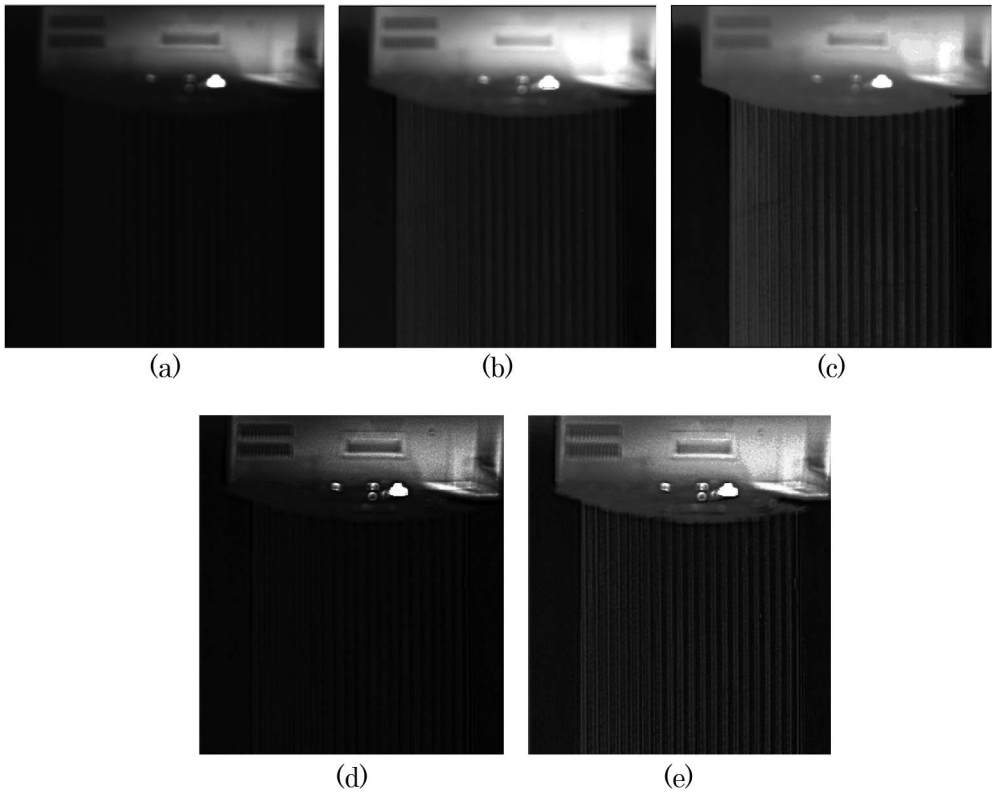

Fig. 8. Experimental results comparison of a door. (a) Original infrared image. (b) Plateau HE. (c) Double plateaus HE. (d) Multiscale new top-hat transform. (e) Proposed algorithm.

In addition, the proposed algorithm can also be applied to enhance other types of images. Figures 10–12 show the visible image, medical image, and lunar surface enhanced by the proposed algorithm.

Figure 10(a) is a visible image. The image is dim, and many details are unclear. HE improves the image contrast, but it produces the overenhancement as shown in Fig. 10(c). After the enhancement, the image contrast is improved, and the image is sharpened. A lot of details become clear such as the dragons.

Figure 11(a) is a medical image, and the edge information is not clear due to the narrow dynamic

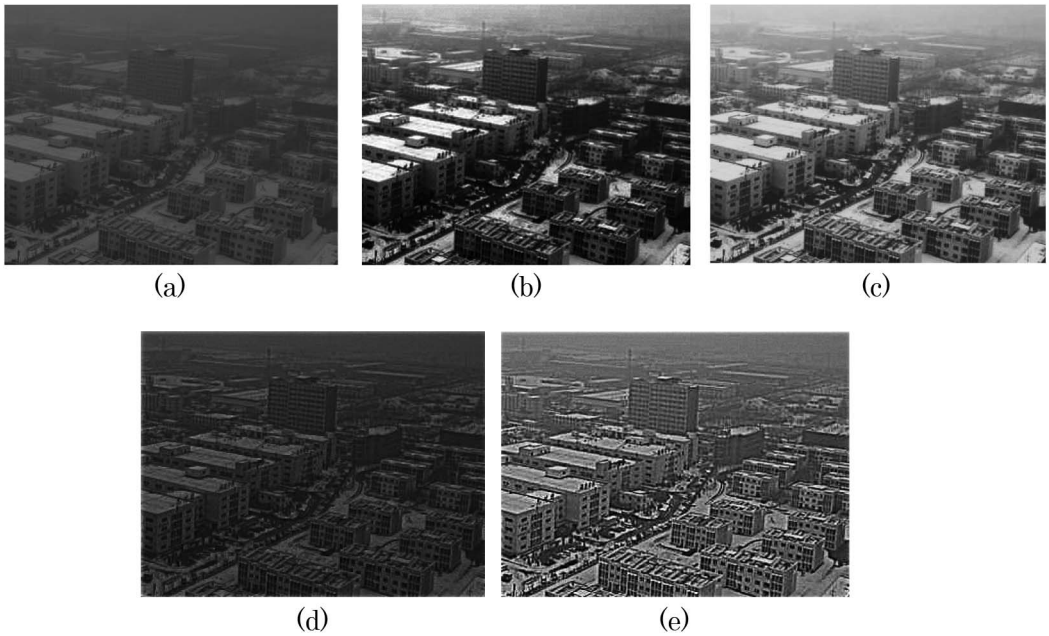

Fig. 9. Experimental results comparison of buildings. (a) Original infrared image. (b) Plateau HE. (c) Double plateaus HE. (d) Multiscale new top-hat transform. (e) Proposed algorithm.

(a) (b) (c)

Fig. 10. Comparison experiment of visible images enhancement. (a) Original image. (b) Proposed algorithm. (c) HE.

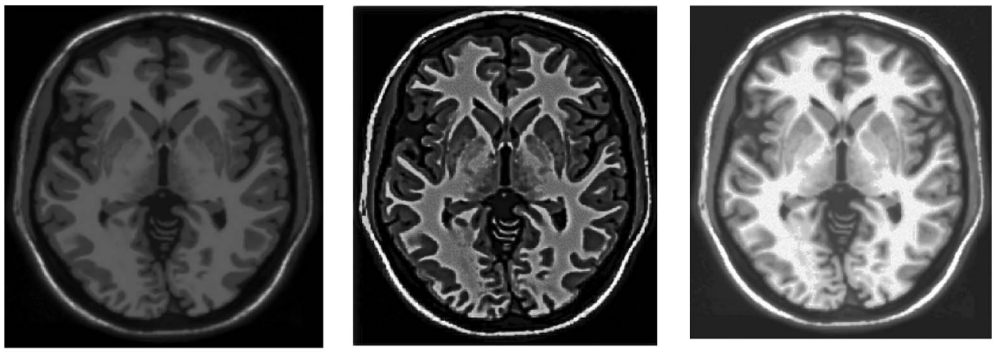

(a) (b) (c)

Fig. 11. Comparison experiment of medical images enhancement. (a) Original image. (b) Proposed algorithm. (c) HE.

range. In Fig. 11(c), HE increases the brightness of the image, but image texture edges are not clear enough. After the proposed algorithm, image details and edges have been well enhanced, and the dynamic range is also expanded.

Figure 12(a) is a lunar surface image, and the edge information is fuzzy. HE expands the dynamic range of the image, but the image has been overenhanced as shown in Fig. 12(c). After the enhancement, the edges have been effectively sharpened, and the image is clear.

The infrared images and other types of images have been applied in the experiment, and the image details and edges are well enhanced, which shows that our algorithm cannot only be applied to effectively enhance infrared images but also can be used to enhance other types of images.

We use the gray mean grads (GMG) for the objective evaluation of image enhancement effect. GMG is defined as follows:

$$\mathrm{GMG} = \frac{1}{(M-1)(N-1)} \sum_{i=1}^{M-1} \sum_{j=1}^{N-1} \sqrt{\frac{(\Delta I_x)^2 + (\Delta I_y)^2}{2}}, \tag{19}$$

where M and N represent the pixel number of the length and width in an image, respectively, ΔI_x and ΔI_y are the gray difference value of adjacent pixels in

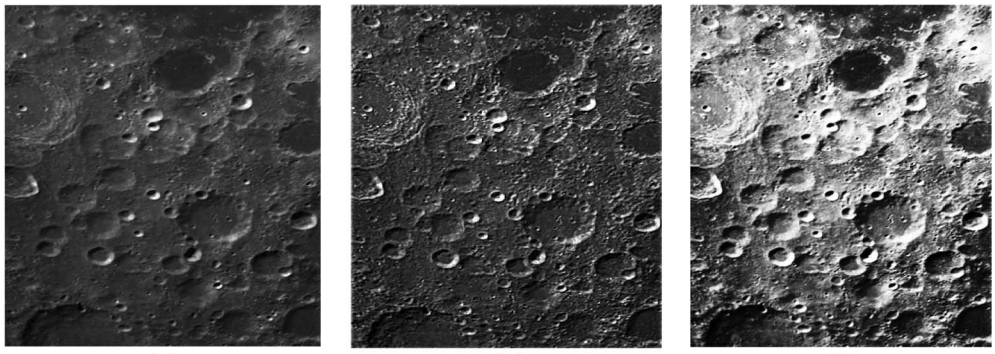

(a) (b) (c)

Fig. 12. Comparison experiment of lunar images enhancement. (a) Original image. (b) Proposed algorithm. (c) HE.

Table 1. Objective Comparison of Image Enhancement Effect Using GMG

	Original Image	Plateau HE	Double Plateaus HE	Multiscale New Top-hat Transform	The Proposed Algorithm
Figure 7	3.639	8.729	11.992	10.230	18.256
Figure 8	1.688	1.874	6.934	6.887	18.927
Figure 9	5.654	10.692	11.825	14.551	26.656

the length and width, respectively. If GMG is bigger, indicating a better performance of image enhancement, the image details and edges are clearer. We calculate GMG of Figs. 7–9 for objective comparison of image enhancement effect by different algorithms, as are listed in Table 1.

In Table 1, plateau HE and double plateaus HE improve the image contrast, and many details are displayed. However, the image edges are unclear. Multiscale new top-hat transform effectively enhance the image edges, but it does not significantly extend the image dynamic range. Compared with the previous three methods, the GMG of the proposed algorithm is the biggest, indicating that it can improve the image contrast and enhance the image details and edges effectively.

4. Conclusion

In this article, we present the infrared image detail enhancement algorithm based on gradient field reconstruction, which can effectively enhance image edge textures and improve contrast. By analyzing the image gradient histogram, we construct a Gaussian function and use it to complete the redistribution of the gradient histogram to enhance weak edge textures of infrared images. In addition, the subhistogram equalization is proposed based on the histogram equalization algorithm to improve the overall contrast of the image. Based on experiment results, the GMG of the original image is improved significantly, and it significantly enhances the faint information and alleviates the edge effects. Therefore, our algorithm cannot only be applied to effectively enhance infrared images but also can be used to enhance other types of images. However, there are some limitations about the algorithm. For infrared images containing large noise, the algorithm cannot obtain good enhancement, which will be further improved in future work.

This work was supported by the National Natural Science Foundation of China (61137001).

References

1. J. J. Talghader, A. S. Gawarikar, and R. P. Shea, "Spectral selectivity in infrared thermal detection," Light Sci. Appl. **1**, 6–16 (2012).
2. K. Choi, C. Kim, M. H. Kang, and J. B. Ra, "Resolution improvement of infrared images using visible image information," IEEE Signal Process. Lett. **18**, 611–614 (2011).
3. V. E. Viekers, "Plateau equalization algorithm for real-time display of high-quality infrared imagery," Opt. Eng. **35**, 1921–1926 (1996).
4. Q. Chen, L. F. Bai, and B. M. Zhang, "Histogram double equalization in infrared image," J. Infrared Millim. Waves **22**, 428–430 (2003).
5. J. A. Ferrari and J. L. Flores, "Nondirectional edge enhancement by contrast reverted low-pass Fourier filtering," Appl. Opt. **49**, 3291–3296 (2010).
6. X. Z. Bai, F. G. Zhou, and B. D. Xue, "Noise-suppressed image enhancement using multiscale top-hat selection transform through region extraction," Appl. Opt. **51**, 338–347 (2011).
7. R. Lai, Y. T. Yang, B. J. Wang, and H. X. Zhou, "A quantitative measure based infrared image enhancement algorithm using plateau histogram," Opt. Commun. **283**, 4283–4288 (2010).
8. K. Liang, Y. Ma, Y. Xue, B. Zhou, and R. Wang, "A new adaptive contrast enhancement algorithm for infrared images based on double plateaus histogram equalization," Infrared Phys. Technol. **55**, 309–315 (2012).
9. M. David, N. Laurent, F. Jacques, and A. Araújo, "Multi-histogram equalization methods for contrast enhancement and brightness preserving," IEEE Trans. Consum. Electron. **53**, 1186–1194 (2007).
10. Q. Wang and K. Ward, "Fast image/video contrast enhancement based on weighted threshold histogram equalization," IEEE Trans. Consum. Electron. **53**, 757–764 (2007).
11. X. Z. Bai, F. G. Zhou, and B. D. Xue, "Infrared image enhancement through contrast enhancement by using multiscale new top-hat transform," Infrared Phys. Technol. **54**, 61–69 (2011).
12. A. Belyaev, "Implicit image differentiation and filtering with applications to image sharpening," SIAM J. Imag. Sci. **6**, 660–679 (2013).
13. C. C. Tseng and S. L. Lee, "Digital image sharpening using fractional derivative and mach band effect," in *International Symposium on Circuits and Systems (ISCAS)* (IEEE, 2012).
14. C. C. Sun, S. J. Ruan, M. C. Shie, and T. W. Pai, "Dynamic contrast enhancement based on histogram specification," IEEE Trans. Consum. Electron. **51**, 1300–1305 (2005).
15. C. Wang and Z. F. Ye, "Brightness preserving histogram equalization with maximum entropy: a variational perspective," IEEE Trans. Consum. Electron. **51**, 1326–1334 (2005).
16. M. Nikolova, Y. W. Wen, and R. Chan, "Exact histogram specification for digital images using a variational approach," J. Math. Imaging Vis. **46**, 309–325 (2013).
17. D. Sen and S. K. Pal, "Automatic exact histogram specification for contrast enhancement and visual system based quantitative evaluation," IEEE Trans. Image Process. **20**, 1211–1220 (2011).
18. W. M. Zuo, L. Zhang, C. W. Song, and D. Zhang, "Texture enhanced image denoising via gradient histogram preservation," in *IEEE Conference on Computer Vision and Pattern Recognition* (IEEE, 2013), pp. 1203–1210.
19. N. Dalal and B. Triggs, "Histograms of oriented gradients for human detection," in *IEEE Computer Society Conference on Computer Vision and Pattern Recognition* (IEEE, 2005), Vol. **1**, pp. 886–893.
20. Y. Z. Zhang, "Improving the accuracy of direct histogram specification," Electron. Lett. **28**, 213–214 (1992).
21. D. A. Socolinsky and L. B. Wolff, "Multispectral image visualization through first-order fusion," IEEE Trans. Image Process. **11**, 923–931 (2002).
22. W. A. A. Wadud, M. H. Kabir, M. A. A. Dewan, and O. Chae, "A dynamic histogram equalization for image contrast enhancement," IEEE Trans. Consum. Electron. **53**, 593–600 (2007).